Sensorless adaptive optics and the effect of field of view in biological second harmonic generation microscopy

Stefaan Vandendriessche, Maarten K. Vanbel and Thierry Verbiest

Molecular Imaging and Photonics, KU Leuven, Celestijnenlaan 200D bus 2425, B-3001 Heverlee, Belgium

ABSTRACT

In light of the population aging in many developed countries, there is a great economical interest in improving the speed and cost-efficiency of healthcare. Clinical diagnosis tools are key to these improvements, with biophotonics providing a means to achieve them. Standard optical microscopy of in vitro biological samples has been an important diagnosis tool since the invention of the microscope, with well known resolution limits. Nonlinear optical imaging improves on the resolution limits of linear microscopy, while providing higher contrast images and a greater penetration depth due to the red-shifted incident light compared to standard optical microscopy. It also provides information on molecular orientation and chirality. Adaptive optics can improve the quality of nonlinear optical images. We analyzed the effect of sensorless adaptive optics on the quality of the nonlinear optical images of biological samples. We demonstrate that care needs to be taken when using a large field of view. Our findings provide information on how to improve the quality of nonlinear optical imaging, and can be generalized to other in vitro biological samples. The image quality improvements achieved by adaptive optics should help speed up clinical diagnostics in vitro, while increasing their accuracy and helping decrease detection limits. The same principles apply to in vivo biological samples, and in the future it may be possible to extend these findings to other nonlinear optical effects used in biological imaging.

Keywords: second harmonic generation, nonlinear optics, microscopy, spatial light modulator

1. INTRODUCTION

In 1961, thanks to the laser, Franken et al. observed the generation of optical harmonics for the first time.[1] Since then, the field of nonlinear optics has come a long way. The symmetry requirements for even order harmonics have lead to their use, amongst others, as fundamental symmetry probes,[2–4] surface characterization tools[5–7] and chirality detection tools.[8–12] Second harmonic generation (SHG) is the most simple even order harmonic, and is the conversion of two photons at frequency ω into a single photon at frequency 2ω. This is equivalent to generating light that has half the wavelength of the incident light; a red laser of 800 nm will generate blue light of 400 nm.[13] The most relevant odd order harmonics for microscopy are third harmonic generation (THG) and two-photon fluorescence (2PF). In THG, three photons of frequency ω combine into a single photon at frequency 3ω.[14,15] 2PF is the absorbance of 2 photons at frequency ω, exciting the molecule to a higher energy level. The molecule subsequently decays back into the ground state via fluorescence with a frequency smaller than 2ω, with the precise frequency depending on many parameters including ω itself, the molecular structure and the dielectric environment.[16–18]

Biological samples are opaque in a large part of the wavelength range relevant for optical microscopy.[19,20] This makes single photon fluorescence challenging in biological samples, as the sample needs to be transparent for both the excitation wavelength and the emission wavelength. In SHG, 2PF and THG microscopy, the excitation and emission wavelengths are more widely separated, making it easier to fulfill this requirement.[20–22] Because these effects depend quadratically or even cubically on the incident light beam intensity, they also focus to a smaller region than linear optical effects, providing the added benefit of higher resolution.[23]

In the ideal case a microscope is diffraction limited, and the resolution of the images depends in first approximation solely on the numerical aperture of the objective and on λ, the wavelength of light.[24] Even in the

Send correspondence to stefaan.vandendriessche@fys.kuleuven.be

case of an ideal microscope, the biological sample itself introduces wavefront distortions. These distortions reduce resolution, but the distortion is inherent to the sample and thus can not be removed from the measurement. The solution is to shape the incident light wavefront such that the wavefront of the light collected from the sample is ideal.[25] Shaping a wavefront has become easier recently with the advent of economical spatial light modulators (SLM).[26] SLMs can be easily controlled using a personal computer, and have the necessary resolution to arbitrarily shape the wavefront of a beam of light. However, in order to correct for wavefront aberrations using an SLM, we need information on the wavefront distortions. This can be either direct knowledge of the distorted wavefront, or indirect information in the form of image quality metrics.[27] Direct knowledge of the distorted wavefront can be acquired by including a wavefront sensor in the experimental setup.[28] When this is not possible or desirable, image quality metrics can be used in order to estimate the distortions or the necessary changes in the incident wavefront in order to improve resolution.[25,29]
Shaping the incident beam's wavefront is achieved by displaying the correct phase pattern on the SLM from which the beam is reflected. However, even for low resolution SLMs, testing every possible phase value for every pixel would take prohibitively long. For this reason, common aberrations are described as a set of orthogonal polynomials called Zernike polynomials, vastly reducing the degrees of freedom in a physically relevant way.[30] The optimal pattern for the SLM is now calculated by superposing the optimized amplitude of each polynomial.

We analyzed the effect of the size of the field of view on the aberration correction in our sensorless nonlinear optical microscope with adaptive optics. Our setup consists of a laser scanning microscope, tuned to 800 nm, an SLM, and no wavefront sensor. Using intensity and sharpness as image quality metrics, we demonstrated that for a large field of view, different areas of the image require different aberration correction. Additionally, we showed that for our samples, sharpness is a more robust image quality metric than intensity for wavefront aberration correction.

2. EXPERIMENTAL DETAILS

Nonlinear optical images were taken on an Olympus BX61WI-FV1200-M system.[31] A Mai Tai DeepSee laser (Newport Spectra Physics) was tuned to 800 nm (120 fs, 82 MHz) and expanded to fill a Holoeye Pluto-NIR-II HR Phase only Spatial Light Modulator (SLM). The beam reflected from the SLM was collimated and aligned into the microscope. The images were recorded with a 15× Thorlabs LMV objective (0.3 NA), and the incident power on the sample was approximately 100 mW. The beam reflected from the sample was split into two beams of equal intensity by a Thorlabs DMLP425R longpass dichroic mirror. The SHG channel was subsequently filtered by a BG39 filter, and 2PF was isolated in the second channel with a Thorlabs FB 400-10 filter. Finally a Hamamatsu R3896 detector detected the non-descanned backward reflection image. This resulted in a 512 × 512 pixel image of a 840 µm × 840 µm region.

The SLM was calibrated using the standard procedure.[32] The laser beam was expanded through a mask consisting of two pinholes, with each spot hitting a different side of the SLM. A webcam was used in order to observe the interference pattern of the reflection of the two spots off of the SLM. By varying the phase of one side of the SLM and correlating this to the observed shift in interference pattern we calibrated the exact phase shift of the SLM.

We used two metrics in order to evaluate the effect of the chosen SLM phase image on the image quality. The first is the intensity, and the second is the sharpness of the image.

$$\text{intensity} = I = \frac{1}{N}\sum_{i}^{N} x_i \tag{1}$$

$$\text{sharpness} = S = \frac{1}{N}\sum_{i}^{N} (I - x_i)^2 \tag{2}$$

where x_i is the value of the ith pixel. For both intensity and sharpness, a larger value was assumed to indicate a better image. A larger intensity is interpreted as more efficient light generation due to better focussing and wavefronts. A higher value for sharpness indicates there are more features present in the image that differ strongly from the average, which is interpreted as better resolved features. Both of these metrics are good indicators of

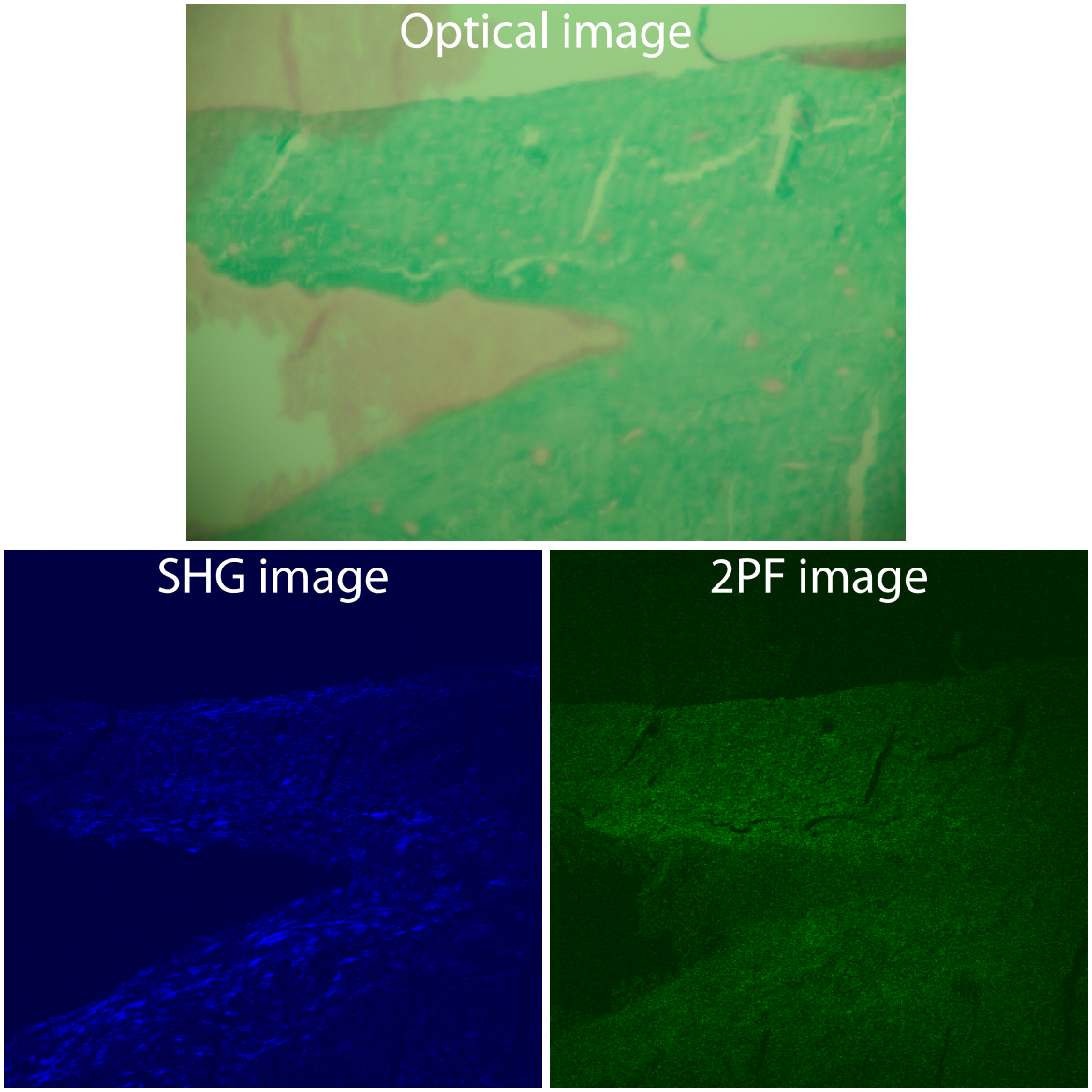

Figure 1. The optical image and false color SHG and 2PF images of 12 week old black 6 J mice tibia, fixated for 24 h at 4 °C with Burckhardt fixative, subsequently dehydrated with 100 % ethanol embedded in methyl methacrylate and then sectioned at 4 µm and stained with Goldner.

image quality for SHG and 2PF biological images, but care needs to be taken when using them for more general sample types.

We used 12 week old black 6 J mice tibia, fixated for 24 h at 4 °C with Burckhardt fixative, subsequently dehydrated with 100 % ethanol embedded in methyl methacrylate and then sectioned at 4 µm and stained with Goldner, as samples.[33–37]

3. RESULTS

We took an optical image of the region of interest of the fixated and stained tibia of 12 week old black 6 J mice (fig. 1), and took SHG and 2PF images of the same region. These images were the initial reference images, used as a starting point in the further wavefront correction analysis. We then applied varying magnitudes of each

Table 1. The Zernike polynomials are a set of orthogonal polynomials that can be used to describe optical aberrations. The first eight polynomials, presented here in the polar coordinate system, describe the most common sources of aberrations in optical microscopes

	formula	common name
Z_1	$\rho\cos\theta$	x tilt
Z_2	$\rho\sin\theta$	y tilt
Z_3	$2\rho^2-1$	defocus
Z_4	$\rho^2\cos 2\theta$	astigmatism, defocus
Z_5	$\rho^2\sin 2\theta$	astigmatism, defocus
Z_6	$(3\rho^2-2)\rho\cos\theta$	coma
Z_7	$(3\rho^2-2)\rho\sin\theta$	coma
Z_8	$6\rho^4-6\rho^2+1$	spherical aberration

Zernike polynomial separately as phase images to the SLM, took images for each magnitude, and analyzed these images. We did this for the first eight Zernike polynomials (table 1).

We evaluated the image quality of the resulting images using sharpness and intensity as image quality metrics. An example is given for the first Zernike polynomial Z_1, "x tilt", in fig. 2. The first conclusion we can draw from our data is that sharpness is a better metric to determine image quality than intensity for our samples. As an example, for the first Zernike polynomial Z_1, the intensity varies a maximum of 5 % in our measurements. In the same images, the sharpness differs by up to 40 %. While both metrics show the same trend and optimum, the changes and exact optimum are clearer when using sharpness as an image quality metric. It has the additional advantage of being less influenced by photobleaching and laser- or setup-induced intensity fluctuations.

A second important conclusion is that for our sample, the optimum for both intensity and sharpness of the first eight Zernike polynomials is the same. This means that a simple single-metric optimization method is sufficient for our samples, and we do not need more complicated optimization methods which weigh different image quality metrics.[29]

The third conclusion concerns the field of view in our microscope. Initially, we optimized for maximal sharpness over the whole image. However, when visualizing the different images (fig. 3), it is clear that the different areas of the image react differently to the different magnitudes of wavefront correction. To quantify this, we divided our image into regions of interest and calculated the intensity and sharpness of each region separately as well as of the whole image. The optima for regions (a) and (c) are similar to, but slightly different from the total image optimum. The optimum for region (b) is clearly different, and lies outside of the measured magnitude of Z_6. This observation can be explained by the large field of view for each image. Biological samples can not be considered uniform over the entire 840 µm × 840 µm region observed by the microscope. Different regions within the field of view will cause different aberrations, and will require different wavefront corrections in order to be visualized optimally.

4. DISCUSSION AND PERSPECTIVES

We analyzed sensorless aberration correction in biological samples, more specifically in mouse tibia. In these samples, we have demonstrated that sharpness is a more robust image quality metric than intensity for sensorless wavefront aberration correction. Despite the fact that sharpness is more robust, sharpness and total intensity lead to the same optimum for all Zernike polynomials tested on our samples. Additionally, in our samples it is sufficient to optimize a single image quality metric to a maximum, demonstrating that for certain sample types it is unnecessary to use more advanced optimization algorithms.
This conclusion is not generalizable to all sample types, as for instance artificial metamaterials behave very differently under a nonlinear optical microscope. Further research is warranted in order to verify to what extent this interesting conclusion applies to other biological samples. We used a very crude metric for image sharpness, but there are many, more refined, metrics that can be used and yield better, possibly more generalizable, results.[38]

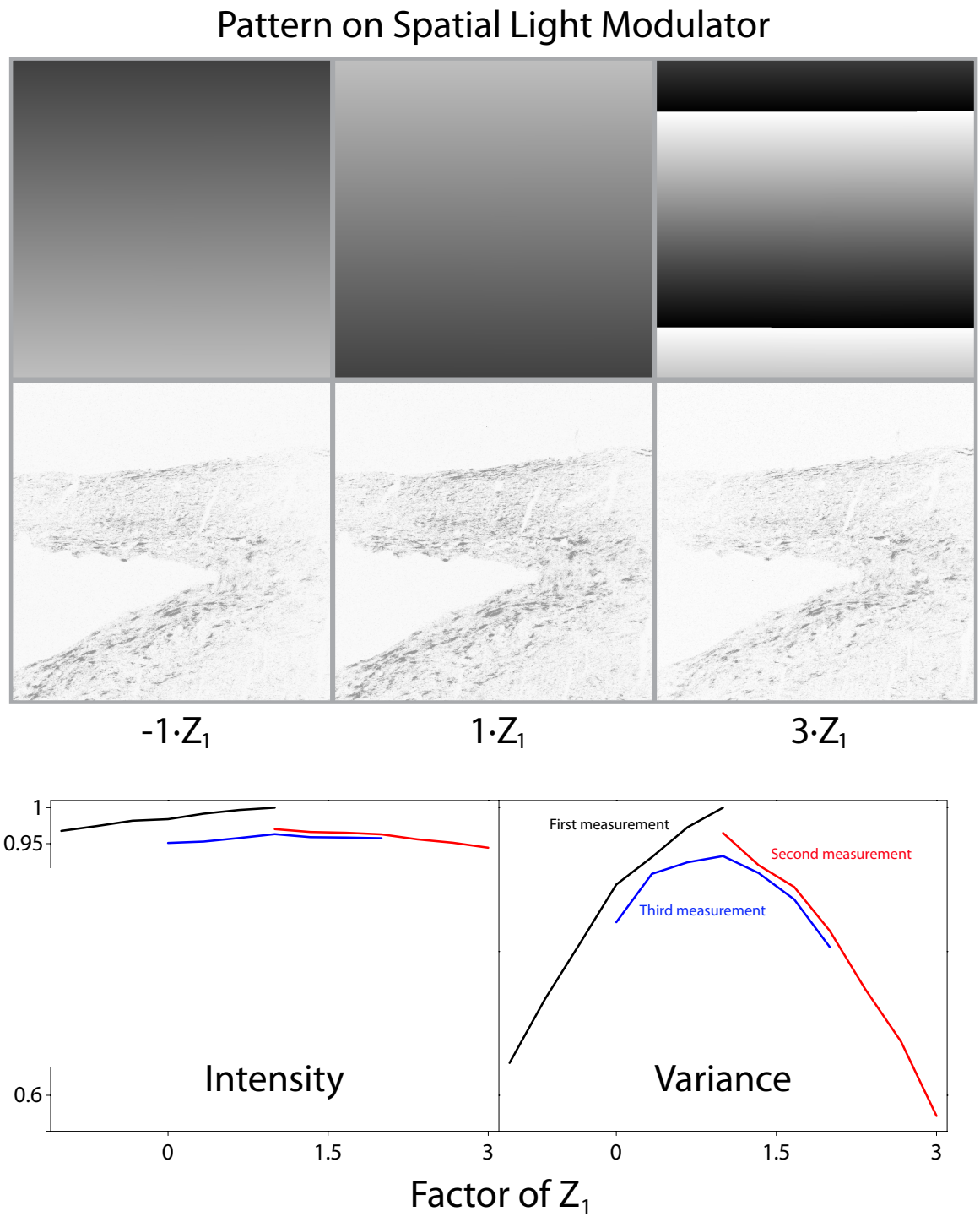

Figure 2. For the first Zernike polynomial Z_1, the intensity varies a maximum of 5 % for the measured SLM phase patterns while the sharpness differs by up to 40 %. We conclude that while both intensity and sharpness show the same trend and optimum, the changes and exact optimum are clearer when using sharpness as an image quality metric. It has the additional advantage of being less influenced by photobleaching and laser- or setup-induced intensity fluctuations.

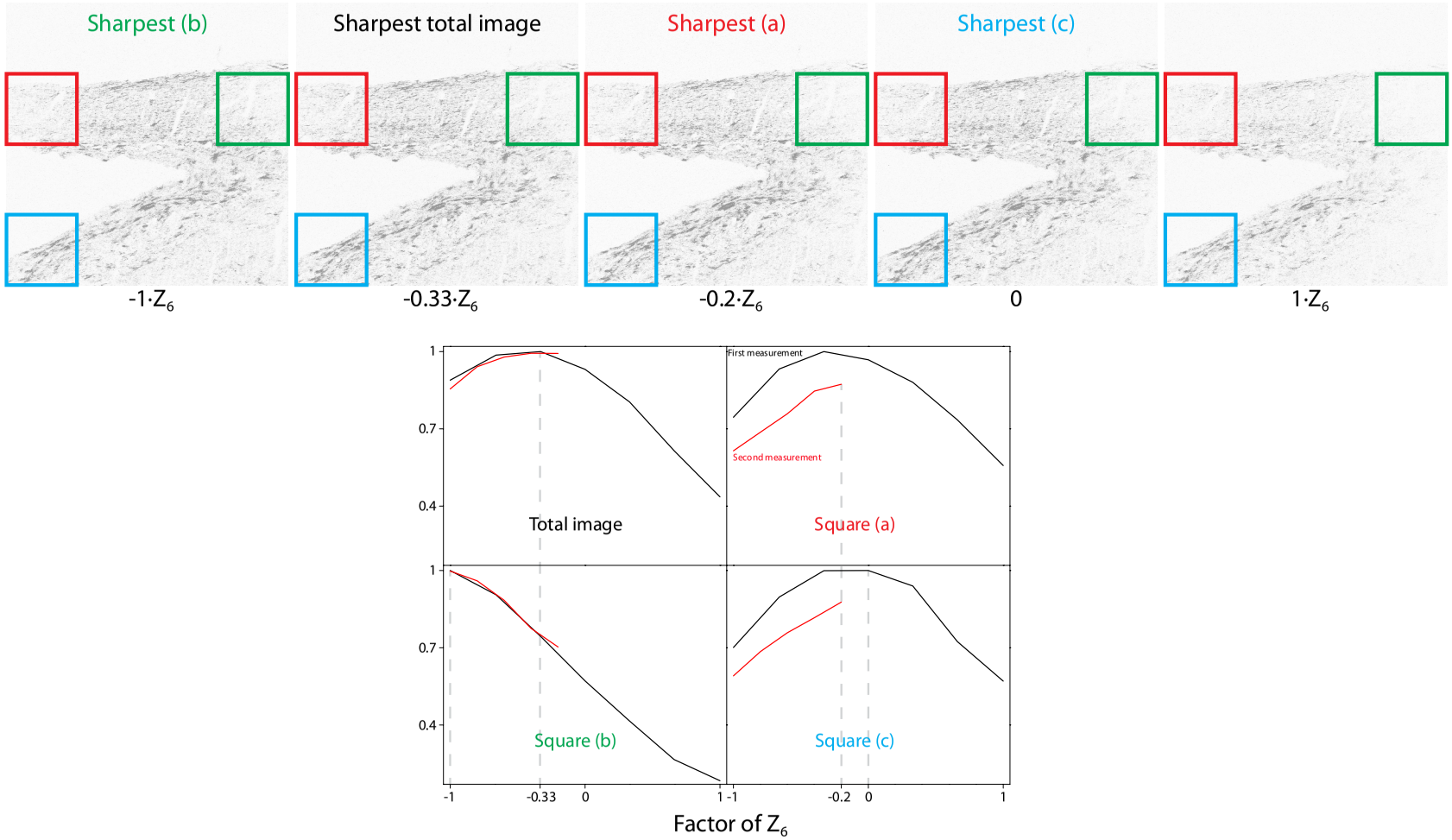

Figure 3. Different areas of the image have different optima for sharpness. This shows that for a large field of view in non-homogeneous samples such as our biological samples, optimizing the entire image will not necessarily have the desired effect, and can result in image quality degradation in certain regions of interest.

We also observed that in the field of view of our images, different regions respond differently to the applied phase patterns. This means that the wavefront aberrations induced by the sample vary significantly over the field of view of our microscope. While an inhomogeneous biological sample is expected to aberrate the wavefront differently in different regions, it is important that these differences are relevant over the field of view of our microscope. This issue can be handled by switching to a technique using wavefront sensing in the setup. If the wavefront sensing is fast enough to cope with the laser-scanning used in the microscope, it is inherently insensitive to this field of view effect. Wavefront sensing nonetheless has a number of drawbacks, including increased cost and system complexity. Maintaining a sensorless technique requires awareness of this field of view effect. It can be diminished by using an objective with a higher magnification or smaller numerical aperture and thus a smaller field of view. If the large field of view is necessary, two choices are available. Whole-image optimization is still possible, and while it will not optimize each region separately, it will result in a higher image quality overall. Alternatively, it is possible to continue imaging the entire field of view, but to only optimize on a single region. This yields the highest quality for the region of interest, while still providing information on the rest of the sample.

ACKNOWLEDGMENTS

Stefaan Vandendriessche is grateful for the financial support from the FWO-Vlaanderen. We are grateful to the University of Leuven (GOA) for financial support. We acknowledge useful discussions with Maarten Bloemen, Ward Brullot and Ventsislav K. Valev.

REFERENCES

[1] Franken, P. A., Hill, A. E., Peters, C. W., and Weinreich, G., "Generation of optical harmonics," *Phys. Rev. Lett.* **7**, 118–119 (1961).

[2] van der Veen, M. A., Vermoortele, F., De Vos, D. E., and Verbiest, T., "Point Group Symmetry Determination via Observables Revealed by Polarized Second-Harmonic Generation Microscopy: (1) Theory," *Anal. Chem.* **84**, 6378–6385 (2012).

[3] Samyn, C., Verbiest, T., Kesters, E., Van den Broeck, K., Van Beylen, M., and Persoons, A., "High glass transition chromophore functionalised poly(maleimide-styrene)s for second-order nonlinear optical applications," *Polymer* **41**, 6049–6054 (2000).

[4] Deckers, S., Vandendriessche, S., Cornelis, D., Monnaie, F., Koeckelberghs, G., Asselberghs, I., Verbiest, T., and van der Veen, M. A., "Poly(3-alkylthiophene)s show unexpected second-order nonlinear optical response," *Chemical Communications* **50**(21), 2741–2743 (2014).

[5] Jordan, D. S., Hull, C. J., Troiano, J. M., Riha, S. C., Martinson, A. B. F., Rosso, K. M., and Geiger, F. M., "Second Harmonic Generation Studies of Fe(II) Interactions with Hematite (α-Fe_2O_3)," *J. Phys. Chem. C* **117**, 4040–4047 (2013).

[6] Vanbel, M. K., Valev, V. K., Vincent, B., Afanas'ev, V. V., Locquet, J.-P., Elshocht, S. V., Caymax, M., and Verbiest, T., "Second-harmonic generation reveals the oxidation steps in semiconductor processing," *J. Appl. Phys.* **111**(6), 064504 (2012).

[7] Vandendriessche, S., Valev, V. K., and Verbiest, T., "Characterization of magnetization-induced second harmonic generation in iron oxide polymer nanocomposites," *Appl. Opt.* **51**, 209–213 (2012).

[8] Huttunen, M. J., Herranen, O., Johansson, A., Jiang, H., Mudimela, P. R., Myllyperkiö, P., Bautista, G., Nasibulin, A. G., Kauppinen, E. I., Ahlskog, M., Kauranen, M., and Pettersson, M., "Measurement of optical second-harmonic generation from an individual single-walled carbon nanotube," *New J. Phys.* **15**(8), 083043 (2013).

[9] Zhu, L. and Cui, Y., "Influence of microscopic parameters of chiral molecules on the first-order hyperpolarizability," *Opt. Commun.* **281**, 170–174 (2008).

[10] Sioncke, S., Van Elshocht, S., Verbiest, T., Kauranen, M., Phillips, K. E. S., Katz, T. J., and Persoons, A., "Circular-difference effects in second-harmonic generation from thin films," *Synthetic Metals* **124**, 191–193 (2001).

[11] Koeckelberghs, G., Vangheluwe, M., Picard, I., De Groof, L., Verbiest, T., Persoons, A., and Samyn, C., "Synthesis and properties of new chiral donor-embedded polybinaphthalenes for nonlinear optical applications," *Macromolecules* **37**(23), 8530–8537 (2004).

[12] Verbiest, T., Kauranen, M., Maki, J. J., Teerenstra, M. N., Schouten, A. J., Nolte, R. J. M., and Persoons, A., "Linearly polarized probes of surface chirality," *J. Chem. Phys.* **103**(18), 8296–8298 (1995).

[13] Verbiest, T., Clays, K., and Rodriguez, V., [*Second-order Nonlinear Optical Characterization Techniques: An Introduction*], CRC Press (2009).

[14] Zhang, Y., Ortega, J., Baumeister, U., Folcia, C. L., Sanz-Enguita, G., Walker, C., Rodriguez-Conde, S., Etxebarria, J., O'Callaghan, M. J., and More, K., "An Azo-Bridged Ferroelectric Liquid Crystal with Highly Enhanced Second and Third Harmonic Generation," *J. Am. Chem. Soc.* **134**(39), 16298–16306 (2012).

[15] Débarre, D., Supatto, W., Pena, A.-M., Fabre, A., Tordjmann, T., Combettes, L., Schanne-Klein, M.-C., and Beaurepaire, E., "Imaging lipid bodies in cells and tissues using third-harmonic generation microscopy," *Nat. Methods* **3**, 47–53 (2006).
[16] Bestvater, F., Spiess, E., Stobrawa, G., Hacker, M., Feurer, T., Porwol, T., Berchner-Pfannschmidt, U., Wotzlaw, C., and Acker, H., "Two-photon fluorescence absorption and emission spectra of dyes relevant for cell imaging," *Journal of Microscopy* **208**(2), 108–115 (2002).
[17] Villa, M. M., Wang, L., Huang, J., Rowe, D. W., and Wei, M., "Visualizing Osteogenesis *In Vivo* Within a Cell–Scaffold Construct for Bone Tissue Engineering Using Two-Photon Microscopy," *Tissue Eng. Pt. C-Meth.* **19**, 839–849 (2013).
[18] Schön, P., Munhoz, F., Gasecka, A., Brustlein, S., and Brasselet, S., "Polarization distortion effects in polarimetric two-photon microscopy," *Opt. Express* **16**, 20891–20901 (2008).
[19] Welsher, K., Sherlock, S. P., and Dai, H., "Deep-tissue anatomical imaging of mice using carbon nanotube fluorophores in the second near-infrared window," *Proceedings of the National Academy of Sciences* **108**(22), 8943–8948 (2011).
[20] Squier, J., Müller, M., Brakenhoff, G. J., and Wilson, K. R., "Third harmonic generation microscopy," *Opt. Express* **3**(9), 315–324 (1998).
[21] Xu, C., Zipfel, W., Shear, J. B., Williams, R. M., and Webb, W. W., "Multiphoton fluorescence excitation: new spectral windows for biological nonlinear microscopy," *Proceedings of the National Academy of Sciences* **93**(20), 10763–10768 (1996).
[22] Masters, B. R. and So, P., [*Handbook of Biomedical Nonlinear Optical Microscopy*], Oxford University Press, USA (2008).
[23] Huang, L. and Cheng, J.-X., "Nonlinear optical microscopy of single nanostructures," *Annual Review of Materials Research* **43**(1), 213–236 (2013).
[24] Pawley, J., [*Handbook of Biological Confocal Microscopy*], Springer (2010).
[25] Emiliani, V., Cojoc, D., Ferrari, E., Garbin, V., Durieux, C., Coppey-Moisan, M., and Di Fabrizio, E., "Wave front engineering for microscopy of living cells," *Optics Express* **13**(5), 1395–1405 (2005).
[26] Bowman, R., D'Ambrosio, V., Rubino, E., Jedrkiewicz, O., Trapani, P., and Padgett, M. J., "Optimisation of a low cost slm for diffraction efficiency and ghost order suppression," *Eur. Phys. J. Special Topics* **199**(1), 149–158 (2011).
[27] Ferzli, R. and Karam, L. J., "A no-reference objective image sharpness metric based on the notion of just noticeable blur (JNB)," *Image Processing, IEEE Transactions on* **18**(4), 717–728 (2009).
[28] Neil, M. A. A., Juškaitis, R., Booth, M. J., Wilson, T., Tanaka, T., and Kawata, S., "Adaptive aberration correction in a two-photon microscope," *Journal of Microscopy* **200**(2), 105–108 (2000).
[29] Nikolenko, V., Watson, B. O., Araya, R., Woodruff, A., Peterka, D. S., and Yuste, R., "SLM microscopy: scanless two-photon imaging and photostimulation using spatial light modulators," *Frontiers in Neural Circuits* **2**(5) (2008).
[30] Noll, R. J., "Zernike polynomials and atmospheric turbulence," *Journal of the Optical Society of America* **66**(3), 207–211 (1976).
[31] Bloemen, M., Vandendriessche, S., Goovaerts, V., Brullot, W., Vanbel, M., Carron, S., Geukens, N., Parac-Vogt, T., and Verbiest, T., "Synthesis and characterization of holmium-doped iron oxide nanoparticles," *Materials* **7**(2), 1155–1164 (2014).
[32] Bergeron, A., Gauvin, J., Gagnon, F., Gingras, D., Arsenault, H. H., and Doucet, M., "Phase calibration and applications of a liquid-crystal spatial light modulator," *Applied Optics* **34**(23), 5133–5139 (1995).
[33] Sinnesael, M., Claessens, F., Boonen, S., and Vanderschueren, D., "Novel insights in the regulation and mechanism of androgen action on bone," *Current Opinion in Endocrinology, Diabetes and Obesity* **20**(3), 240–244 (2013).
[34] Sinnesael, M., Callewaert, F., Morreels, M., Kumar, N., Sitruk-Ware, R., Van Proeyen, K., Hespel, P., Boonen, S., Claessens, F., and Vanderschueren, D., "7α-methyl-19-nortestosterone vs. testosterone implants for hypogonadal osteoporosis: a preclinical study in the aged male orchidectomized rat model," *International Journal of Andrology* **34**(6pt2), e601–e611 (2011).
[35] Sinnesael, M., Claessens, F., Laurent, M., Dubois, V., Boonen, S., Deboel, L., and Vanderschueren, D., "Androgen receptor (AR) in osteocytes is important for the maintenance of male skeletal integrity: Evidence from targeted AR disruption in mouse osteocytes," *Journal of Bone and Mineral Research* **27**(12), 2535–2543 (2012).
[36] Callewaert, F., Sinnesael, M., Gielen, E., Boonen, S., and Vanderschueren, D., "Skeletal sexual dimorphism: relative contribution of sex steroids, GH–IGF1, and mechanical loading," *Journal of Endocrinology* **207**(2), 127–134 (2010).
[37] Sinnesael, M., Boonen, S., Claessens, F., Gielen, E., and Vanderschueren, D., "Testosterone and the male skeleton: A dual mode of action," *Journal of Osteoporosis* **2011**, 240328 (2011).
[38] Moreno, P. and Calderero, F., "Evaluation of sharpness measures and proposal of a stop criterion for reverse diffusion in the context of image deblurring," in [*VISAPP (1)*], 69–77 (2013).